Nanoscale

PAPER

View Article Online
View Journal | View Issue

Check for updates

Cite this: *Nanoscale*, 2025, **17**, 5150

Mixed metal halide perovskite $CsPb_{1-x}Sn_xBr_3$ quantum dots: insight into photophysics from photoblinking studies†

Anusha A,[a] Anjali Yadav,[a] Pratap Vishnoi[b] and Dharmendar Kumar Sharma *[a]

Mixing different metal ions at the B site of ABX_3 perovskites offers a promising approach for addressing challenges related to toxicity, stability and performance in optoelectronic applications. One such example is $CsPb_{1-x}Sn_xBr_3$ which addresses the toxicity issue posed by lead while allowing us to tune optoelectronic properties such as the band gap. In this work, nearly monodisperse $CsPb_{1-x}Sn_xBr_3$ quantum dots (QDs) were synthesized with variable Pb/Sn compositions, *i.e.* $CsPbBr_3$, $CsPb_{0.9}Sn_{0.1}Br_3$ and $CsPb_{0.7}Sn_{0.3}Br_3$. The photoluminescence quantum yield (PLQY) of $CsPb_{1-x}Sn_xBr_3$ first increases for $x = 0.1$ and then decreases for $x = 0.3$ with respect to $x = 0$. Such an effect of Sn incorporation on the PLQY was investigated using photoblinking studies which revealed three levels of blinking statistics namely ON, GRAY and OFF. These results along with the excited state lifetime measurements enabled us to understand charge carrier dynamics in the $CsPb_{1-x}Sn_xBr_3$ QDs. Based on our findings, we propose that the photogenerated hot electrons of Sn enhance the PLQY by filling the trap states centered on Pb, which otherwise promote non-radiative relaxations in the Sn-free $CsPbBr_3$. However, at higher Sn concentrations, non-radiative recombination becomes more pronounced, reducing the PLQY.

Received 20th November 2024,
Accepted 16th January 2025

DOI: 10.1039/d4nr04879b

rsc.li/nanoscale

Published on 17 January 2025. Downloaded on 2/15/2026 1:56:55 AM.

Introduction

Lead halide perovskites (LHPs) have gained prominence as materials with exceptional optoelectronic properties, characterized by their remarkable photoluminescence efficiency, long carrier diffusion lengths and efficient charge transport.[1–5] Such properties enabled them to be useful materials for the advancement of efficient, low-cost, and scalable devices for solar cells, light emitting diodes (LEDs) and various other optoelectronic applications.[6–9] The distinctive crystal structure of LHPs is denoted as ABX_3, where A is a monovalent cation (*e.g.*, Cs^+, Rb^+, CH_3–NH_4^+, *etc.*),[10] B is a divalent metal cation (*e.g.*, Pb^{2+}, Sn^{2+}, *etc.*), and X is a halide anion (*e.g.*, Cl^-, Br^-, I^-, *etc.*).[11–13] These ions contribute to the optoelectronic characteristics of LHPs and allow for fine control over the bandgap, enabling the design of perovskite materials for specific applications.[6,11,14] Despite the excellent optoelectronic properties of LHPs, the eco-toxicity of Pb^{2+} and stability are serious concerns for their large-scale applications.[15] Complete replacement of Pb by Sn in lead-free perovskite halides (LFPHs), *i.e.*, $CsSnX_3$, yields very low PL quantum efficiency due to the rapid oxidation of Sn(II) to Sn(IV) that enhances lattice instabilities and trap-assisted recombination.[16–19] Alternatively, partial substitution of Pb by Sn, Zn, Mn, Bi, *etc.* was suggested by different groups to reduce the Pb content in LHPs.[20–26] It is observed that the photoconversion efficiencies of LHPs are enhanced significantly when Pb was partially substituted by Sn.[20] Subsequently, perovskite nanocrystals of mixed metal cations with varying Pb(II) and Sn(II) ratios have been developed for applications in LEDs.[20,27,28] Interestingly, it is noted that a certain amount of Sn enhances the photoluminescence quantum yield (PLQY) which decreases upon a further increase in the amount of Sn. The presence of Sn in these materials has been confirmed both on the surface and within the bulk; hence the observed change in PLQY with increasing Sn content cannot be solely attributed to surface passivation effects.[19,27] The way Sn affects the electronic transitions and the photophysical properties of these mixed metal perovskite halides, *i.e.*, $CsPb_{1-x}Sn_xBr_3$, remains unclear and largely unknown. The changes in Sn content may alter the crystal structure, phase segregation or the electronic environment, which can affect the charge carrier dynamics and radia-

[a]*Department of Chemistry, Maulana Azad National Institute of Technology, Bhopal-462003, India. E-mail: drdksharma@manit.ac.in; Tel: +755-2671660*
[b]*New Chemistry Unit, International Centre for Materials Science, Jawaharlal Nehru Centre for Advanced Scientific Research, Jakkur P.O., Bangalore-560064, India*

†Electronic supplementary information (ESI) available: Materials and synthesis methodology, EDS spectra and data table of $CsPb_{1-x}Sn_xBr_3$ QDs, Tauc plot of $CsPb_{1-x}Sn_xBr_3$ QDs, home-built spectral imaging setup, histogram of the spatial distribution of PL, examples of the intensity traces of $CsPb_{1-x}Sn_xBr_3$ QDs, and criteria for determining ON, GRAY, and OFF states (PDF). See DOI: https://doi.org/10.1039/d4nr04879b

This journal is © The Royal Society of Chemistry 2025

Published on 17 January 2025. Downloaded on 2/15/2026 1:56:55 AM.

tive recombination processes responsible for PL.[27] In general, such an unusual PLQY trend is illustrated by defect state mechanisms involving different processes of charge carrier dynamics[28] corroborated by biexciton and trion lifetimes.[20] Nonetheless, it is crucial to understand the impact of Sn on the electronic transitions and photophysical properties of these partially substituted mixed metal LHPs. Photoblinking studies can provide a detailed, single-particle perspective of the processes affecting the PLQY in the partially substituted LHPs that are not accessible through bulk measurements.

Photoblinking is a complex phenomenon resulting from the radiative and non-radiative recombination of excitons at different time intervals under continuous excitation. Several theoretical models such as Auger ionization, trapping/de-trapping, multiple recombination center (MRC), quantum mechanical tunneling of charge carriers, *etc*. have been developed to comprehend photoblinking behavior.[29,30] In terms of two-state blinking, the radiative recombination events are called the ON-time, while the nonradiative recombination events are called the OFF-time. Depending on the PL intensity and lifetime, photoblinking is classified majorly by two distinct types: (i) A-type, charging and discharging of QDs where a low PL intensity is accompanied by a low excited state lifetime and (ii) B-type, a large change in PL intensity with no change in PL lifetime because of the existence of electron-accepting sites on the surface; when unoccupied, they accept hot electrons/carriers prior to relaxation (HC-blinking).[31] Another type, *i.e.*, BC type blinking, has also been recognized where the PL intensity decreased linearly with lifetime and is explained by non-radiative fluctuations in the rates due to activation and deactivation of the transient surface traps.[29] In the charging model, an electron or hole is confined in a deep level/trap state, resulting in the formation of a trion (when a new carrier is combined with a pair of carriers and forms a total of three carriers). This trion mainly undergoes non-radiative recombination, contributing to OFF-time. However, the MRC model illustrates that multiple shallow levels are activated and deactivated alternatively, promoting the non-radiative recombination of excitons and ultimately causing OFF-time by the activated shallow levels.[30] Photoblinking in perovskites has been studied at different extents to understand the effect of charge trapping, ligand exchange,[32] electric field and varied environmental spatiotemporal correlation.[33,34] However, changes in photoblinking behavior due to Sn substitution in LHPs have not yet been reported.

In this report, we focus on understanding the PL properties of $CsPb_{1-x}Sn_xBr_3$ QDs with different amounts of Sn. We have chosen $CsPb_{1-x}Sn_xBr_3$ QDs of ~6–9 nm size, smaller than twice the Bohr exciton radius (5.5 nm for $CsPbBr_3$), *i.e.*, in a strong quantum confinement regime,[35] and performed photoblinking experiments on individual $CsPb_{1-x}Sn_xBr_3$ emitters of three different compositions (for x = 0, 0.1 and 0.3). Three-step photoblinking behavior, namely, ON, GRAY and OFF states, analysis allows us to correlate the observed PL characteristic with the extent of Sn substitution. Based on ensemble and single-particle investigations, we discuss the origin of the unusual PL trend observed with increasing Sn amount. We show that PL enhancement for a small fraction of Sn in the $CsPb_{1-x}Sn_xBr_3$ QDs is due to the suppression of GRAY states which is facilitated by the hot electrons from Sn. These electrons occupy the surface trap states of Pb(II) and inhibit the transition of excited electrons from the conduction band (C.B.) to the non-radiative recombination centers. However, a further increase in the number of Sn hot electrons and the proximity of Sn results in undesired interactions, which is reflected in a significant modification of the photo-blinking behavior. Overall, the suitable Sn content leads to a higher fraction and longer duration of ON-times at the expense of GRAY states, while an excess amount of Sn results in a significant increase in the fraction and duration of OFF-times.

Experimental

Mixed metal halide perovskite synthesis

$CsPb_{1-x}Sn_xBr_3$ QD_s with varying x values of 0, 0.1 and 0.3 (named hereafter) were synthesized with slight modifications using the hot injection method.[11] To vary the fraction of Sn substitution, stoichiometric ratios of their respective precursor components varied with no other change in the reaction conditions. Details of the synthesis and experimental methods are provided in the ESI.†

Structural and morphological characterization

Diluted $CsPb_{1-x}Sn_xBr_3$ dispersed in toluene was sonicated and drop-cast (100 μL) onto carbon-supported copper grids and subsequently dried overnight under vacuum. HRTEM imaging and EDS were performed using a Thermo Fisher Talos F200 S operated at 200 kV. The size distribution (Fig. 1a–c) of the synthesized $CsPb_{1-x}Sn_xBr_3$ perovskites was determined using Image J and the elemental composition (Fig. S1–S3†) was obtained from the atomic fraction percentage (Table S1†). HRTEM images were analysed to obtain d-spacing using GATAN software (Fig. 1d–f).

Absorption, PL emission and relative PLQY measurements

UV–vis absorption and PL emission spectra were recorded using a PRIZM ABS-UV-VIS spectrophotometer. The band gap energy was estimated using the Tauc plot (Fig. S4†). For PL, a 405–410 nm excitation source was used to excite the $CsPb_{1-x}Sn_xBr_3$ dispersed in toluene. The relative PLQY was measured using perylene fluorescent dye.[32] Information on the spectral peak positions and FWHM (full width at half-maximum) for the PL spectra was obtained using Gaussian function fitting.

Excited state lifetime measurements

A TCSPC Edinburgh Instruments (FLS 1000) equipped with a cryostat (13k–400k) was used to record the excited state decay curves of the $CsPb_{1-x}Sn_xBr_3$ dispersed in toluene. The lifetime decay curves obtained at λ_{exc} = 405 nm were fitted with the bi-

Published on 17 January 2025. Downloaded on 2/15/2026 1:56:55 AM.

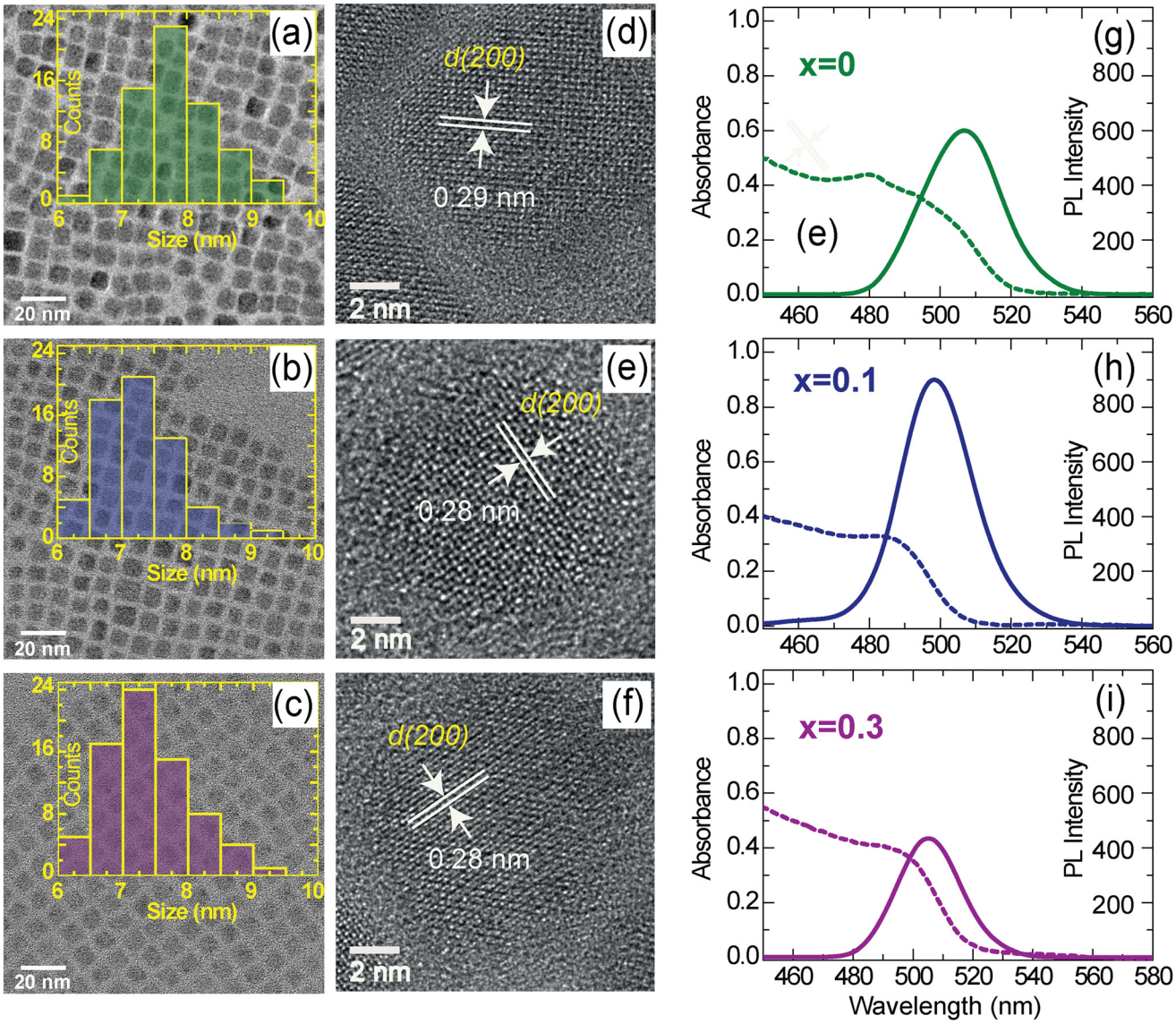

Fig. 1 TEM images with respective size distributions overlaid on each image (a–c) and the corresponding HRTEM images (d–f). The marked *d*-spacing of 0.29 nm corresponds well with the (200) crystallographic plane of cubic phase $CsPbBr_3$, while for $x = 0$ and $x = 0.3$, this *d*-spacing was determined to be 0.28 nm. Steady-state absorption (dotted line, g–i) and optical density (OD)-corrected PL spectra (solid line, g–i) of different $CsPb_{1-x}Sn_xBr_3$ QDs with varying $x = 0$ (a, d, and g), $x = 0.1$ (b, e, and h), and $x = 0.3$ (c, f, and i). Histograms are colour coded with the spectra shown in the right panel (g–i).

exponential decay function to obtain two different lifetimes and their respective fractions.

Single-particle photoblinking studies

Single-particle PL imaging of the $CsPb_{1-x}Sn_xBr_3$ perovskite was performed using a home-built fluorescence microscope setup in epifluorescence mode, as shown in Fig. S5.† Photoblinking samples were prepared by spin-coating ~ nM suspensions of $CsPb_{1-x}Sn_xBr_3$ in toluene at 1500 rpm for 60 s onto 24 × 24 mm micro cover glass (Matsunami, Japan). All the samples were dried under vacuum before mounting on the microscope. The sample was mounted on an inverted microscope (Olympus (IX73)) equipped with excitation sources (Fig. S5†). A 405 nm laser (DPPS, 405-LM-100T) was used to excite (at a constant power of 300 μW, measured just before the objective lens) the sample through a 60× objective lens (1.51 NA, oil immersion, Olympus) in epifluorescence mode. Emerging PL was separated from laser excitation using a 405 nm long pass dichroic 450 nm notch filter. A CMOS camera with 2040 × 2040 resolution (PCO.PANDA 4.2) was used as a detector to record the data in movie format at a frame rate of 50 fps for photoblinking analysis. Control experiments were performed to optimize the workable concentration of the individual emitters within the region of interest. Care has been taken to consider the well separated (by ≥500 nm) emitters for further analysis.

This journal is © The Royal Society of Chemistry 2025

Published on 17 January 2025. Downloaded on 2/15/2026 1:56:55 AM.

Data analysis

Single-particle image frames obtained in movie formats were analysed as reported in the reference.[33,36] In brief, freely available ImageJ (NIH) software was used for image processing and extracting PL intensity time traces for individual emitters. The intensity time trajectories ("*z*-profile" in ImageJ) were acquired by making a 3 × 3-pixel ROI on well-separated emission spots. The acquired data were exported in ASCII format for further analysis using MATLAB 2020 to construct PL intensity probability distributions, shadows, *etc*. Data fitting and plotting were performed using MATLAB and QtiPlot.

Results and discussion

Structure and morphology of $CsPb_{1-x}Sn_xBr_3$ QDs

TEM images of the $CsPb_{1-x}Sn_xBr_3$ QDs (x = 0, 0.1 and 0.3) are shown in Fig. 1(a–c). All three samples exhibited nearly monodisperse nano cubes, suggesting a similar growth mechanism for the three samples. The size distributions histograms of these nanocubic QDs show size in the range of 6–9 nm (Fig. 1a–c, insets). Further, the presence of characteristic peaks corresponding to Cs, Pb, Br and Sn (for x = 0.1 and 0.3) in the energy dispersive X-ray (EDX) spectra validate their successful incorporation in the QDs in the desired stoichiometry (Fig. S1–S3 and Table S1†). Although the size of these nano cubes falls in the quantum confinement regime, similar sizes and ratios of Sn and Pb in proportion to their presence in reaction media allowed us to compare their optoelectronic properties comprehensively where the influence of composition is expected. Furthermore, high-resolution TEM images have been acquired to investigate their crystalline nature and phase purity (Fig. 1d–f). For x = 0, the interplanar distance (*i.e.*, *d*-spacing) is observed as 0.29 nm, which corresponds to the (200) crystallographic plane of cubic phase $CsPbBr_3$ (ICSD-29073).[13,37] For the x = 0.1 and x = 0.3, we observed a slightly decreased *d*-spacing of 0.28 nm, indicating the incorporation of Sn without changing the parent structure of the $CsPbBr_3$ QDs. This slight contraction of the lattice is a consequence of Sn^{2+} incorporation in place of Pb^{2+} ions. Consistent *d*-spacing and uniform lattice fringes indicates the absence of significant structural change or phase segregation across the investigated Sn concentrations in the $CsPb_{1-x}Sn_xBr_3$ QDs.[22]

Steady-state absorption and photoluminescence measurements

The optical properties of the synthesized materials dispersed in toluene were investigated using absorption and PL emission measurements (Fig. 1g–i). The absorption spectra of the $CsPb_{1-x}Sn_xBr_3$ QDs are broad with no discernible absorption peaks (Fig. 1g–i, dotted line), irrespective of the x values. The bandgaps of the synthesized $CsPb_{1-x}Sn_xBr_3$ QDs estimated using the Tauc plot (Fig. S4†) were found to be 2.48 eV (x = 0), 2.51 eV (x = 0.1) and 2.49 eV (x = 0.3). PL spectra obtained for the same sample(s) are presented in (Fig. 1g–i, solid lines), these spectra show PL maxima (λ_{max}^{PL}) at ~506 nm (2.45 eV), ~498 (2.49) nm and ~504 (2.46) nm for x = 0, x = 0.1 and 0.3 respectively. The Stokes shift determined from absorption and PL emission varies from 20 to 30 meV. The OD-corrected PL intensity in a small fraction of the Sn (x = 0.1) sample demonstrates enhanced PL efficiency as compared to the x = 0 sample, along with a blue shift of ~8 nm of λ_{max}^{PL} as shown in Fig. 1g–h. Further increase in the fraction of Sn (x = 0.3) led to a decrease in the PL intensity while λ_{max}^{PL} shifts close to the λ_{max}^{PL} of x = 0 (Fig. 1i). To get clarity on unusual changes in the PL behaviors, the PLQY of all three samples were estimated using perylene as a reference.[32] The PLQY of $CsPb_{1-x}Sn_xBr_3$ for x = 0 was found to be ~71%, which increases to 89% for x = 0.1 and then decreases to 53% for x = 0.3. We note that for x = 0 → x = 0.1, a small fraction of Sn (*i.e.* x = 0.1) may aid in enriching the perovskite surface by acting as a self-passivation layer.[20,27,28] However, the decrease in intensity with further increase of Sn (from x = 0.1 → x = 0.3) cannot be explained merely by accounting for such self-passivation by Sn.[27] Such a change in the PLQY can be attributed to the presence of an appropriate amount of Sn that may enhance the optical efficiency either by fostering the radiative recombination or by suppressing the non-radiative pathways. To get further insight into the way how Sn incorporation affects the emission intensity, experiments were performed at the single-particle level which uncovers the details masked in bulk experiments due to number and time averaging effects.

Single-particle photoblinking studies

Single-particle PL imaging of the $CsPb_{1-x}Sn_xBr_3$ QDs was performed on a home-built spectral imaging setup under 405 nm excitation, experimental setup (Fig. S5†) and analysis methods are presented in the Experimental section. Time averaged single-particle images of the $CsPb_{1-x}Sn_xBr_3$ QDs for different 'x' values are shown in Fig. 2(a–c) where individual emitters appeared as bright spots over a dark background. From such averaged over the time images of all three samples, the spatial distribution of intensity created (Fig. S6†), suggesting that the $CsPb_{1-x}Sn_xBr_3$ QDs with x = 0.1 are brighter as compared to those with x = 0 and x = 0.3. Representative intensity time traces from the individual $CsPb_{1-x}Sn_xBr_3$ QD (two examples from each sample) emitters of different Sn contents are shown in Fig. 2(d–f), along with the distribution of the population at different intensity levels in terms of frequencies of their occurrence. These histograms show how intensity is distributed at different levels for the given intensity traces in Fig. 2(d–f). More such intensity time traces for all three samples are given in Fig. S7.† It should be noted from Fig. 2(d–i) that the intensity fluctuations show different levels, *i.e.*, transitions between high intensity 'ON' states, background level intensity 'OFF' states and intermediate (dim) states referred to as GRAY states hereafter. To generate the statistical relevance of the observed behavior, the intensity trajectories of 56 (for x = 0), 63 (for x = 0.1) and 48 (for x = 0.3) $CsPb_{1-x}Sn_xBr_3$ QDs were analyzed and discussed later. The multistep blinking behavior was analyzed using two different thresholds as reported elsewhere.[33] The ON and OFF intensity levels are discriminated by $\langle I_{ON} \rangle \pm 2\sigma$

Published on 17 January 2025. Downloaded on 2/15/2026 1:56:55 AM.

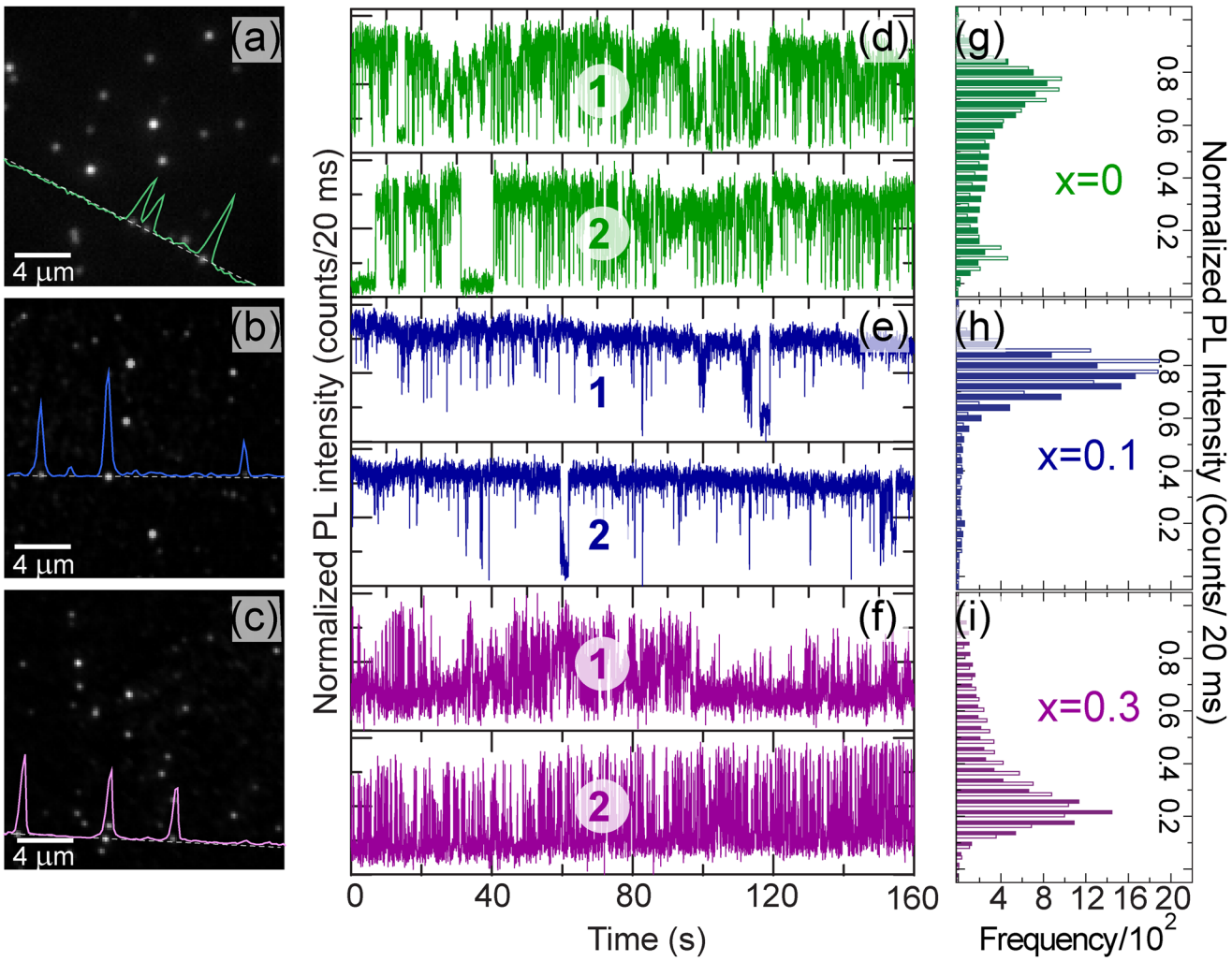

Fig. 2 Time averaged single-particle PL images (a–c), intensity line profiles (solid lines) for the spatial region (dotted line) are shown to depict brightness (signal to noise) and physical separations between the nearby emissive spots. Representative PL intensity (normalized) time traces from individual emitters (d–f) (shown for the two particles marked 1 and 2) and intensity distributions (g–i) (shown for the two particles marked 1 and 2) in (d–f) for $CsPb_{1-x}Sn_xBr_3$ QDs with varying x = 0 (d, g), x = 0.1 (e, h), and x = 0.3 (f and i). Line profiles, intensity time traces and intensity histograms are color coded for visual aids.

and $\langle I_{OFF}\rangle \pm 2\sigma$, where I_{ON} and I_{OFF} are the intensities of the ON and OFF levels and σ is the standard deviation from the mean, *i.e.* noise (Fig. S8†). The intensity values which do not fall under the above criteria are termed GRAY states. Such GRAY states have frequently been observed under high density excitation for group II–IV nanocrystals (NCs) and linked with the emission from charged states.[38,39] For perovskite NCs, these GRAY states are known even at low excitation densities.[33,40] These GRAY states are thought to arise from fast mixing and time averaging of ON (neutral, emissive) and OFF (charged, quenched) states. Alternatively, emission arising from a charged excited state is known as trions that relax partly non-radioactively and may result in the intermediate intensity *i.e.*, GRAY states.

Nonetheless, irrespective of the origin, the frequency of GRAY states decreased from x = 0 to x = 0.1 which in turn enhances the average intensity (brightness) of individual emitters. In contrast, OFF states are relatively more frequent for x = 0.3 as compared to the former two samples. To obtain quantitative information, the intensity traces of individual $CsPb_{1-x}Sn_xBr_3$ QDs with different 'x' values were analyzed statistically in terms of probability density distributions of separate levels: $\left(P(t_i) = \frac{2N_{t,i}}{(t_{i+1} - t_i) + (t_i - t_{i-1})}\right)$ and their particular fractional times: $T^{FR}_{ON(\text{or OFF or GRAY})} = \frac{\sum_N t^{ON(\text{or OFF or GRAY})}}{\sum_N t^{ON} + \sum_N t^{OFF} + \sum_N t^{GRAY}} \times 100$; where N is the occurrence and t is the period for the particular event.

Distributions of the time fractions of ON, GRAY, and OFF states for all three samples were compared and are presented

 This journal is © The Royal Society of Chemistry 2025

Published on 17 January 2025. Downloaded on 2/15/2026 1:56:55 AM.

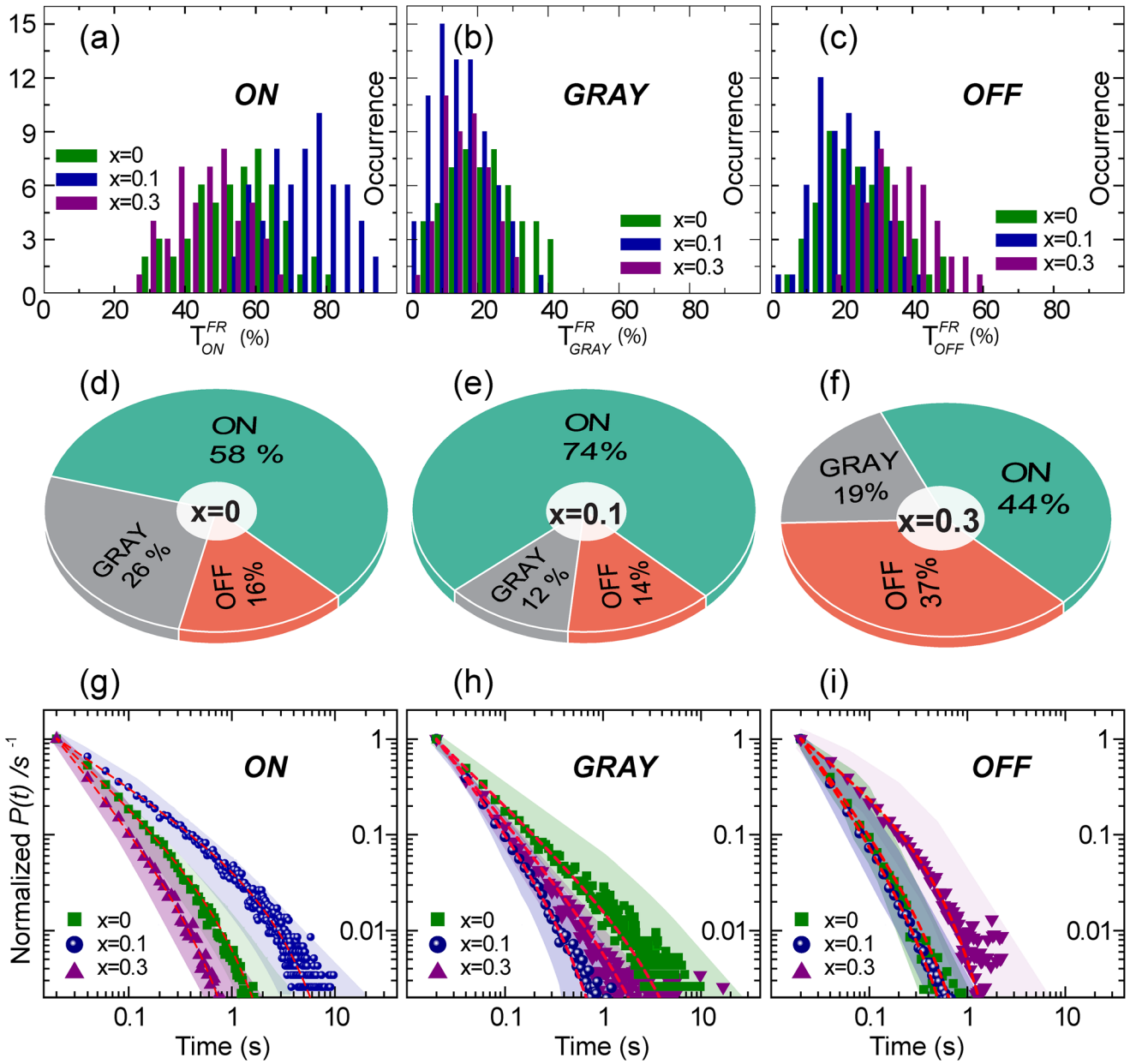

Fig. 3 Distribution(s) of fractional times for ON, OFF and GRAY states (a–c). To understand the ON, GRAY and OFF times for individual samples, pi-charts are provided (d–f). Comparison of probability density ($P(t)$) distributions for ON (g), GRAY (h) and OFF (i) times for $CsPb_{1-x}Sn_xBr_3$ QDs (g–i). These $P(t)$ plots represent ensemble averages; these are derived from the sum of a large amount of data across multiple QDs. All ($P(t)$) data were fitted with the truncated power law (red dotted line). The extent of variation in 'α' and the truncation time are shown as shadows overlaid over each $P(t)$ plot of combined particles as discussed in the main text. Each histogram, $P(t)$ curves and shadows are color coded to enhance understanding.

in Fig. 3(a–c). For clarity, the percentage contributions of ON, GRAY, and OFF events are shown separately for each sample in Fig. 3(d–f) as pi-charts. These pi-charts show enhanced ON (58% to 74%), suppressed GRAY (26% to 12%) and comparable OFF (16% to 14%) fractions for $x = 0$ to $x = 0.1$. This indicates that mainly the ON states for $x = 0.1$ switched from the GRAY states for $x = 0$. This in turn resulted in an enhanced PLQY for $x = 0.1$. In contrast, the decrease in the PLQY for the $x = 0.3$ sample is mainly due to the increased OFF durations (14% to 37%) in relation to the $x = 0.1$ sample, although increased GRAY states (19%) also impact the PLQY negatively. The probability density ($P(t)$) curves of "ON", "GRAY" and "OFF" times for three different samples are plotted as a double logarithmic graph, as shown in Fig. 3(g–i). We note that ($P(t)$) curves at long time durations exhibit exponential probability that cannot be accounted by the simple power law. Therefore, the truncated power law function ($P(t) = At^{-\alpha}e^{-t/t_c}$) was used to fit ($P(t)$) curves to account for the truncation occurring at long-time events. In this equation, α is the exponent (corresponds to the slope) which increases with the decreasing period of the

Published on 17 January 2025. Downloaded on 2/15/2026 1:56:55 AM.

given event, while t_c indicates the critical time, *i.e.*, the time when the power law function is dominated by the exponential function.[32,41] The fitting results in terms of α and t_c for the ON, GRAY and OFF states for different 'x' values of the $CsPb_{1-x}Sn_xBr_3$ QDs are presented in Table 1.

For ON times, α decreases from 1.01 for $x = 0$ to 0.73 for $x = 0.1$ which indicates the enhanced periods of the ON states for the given amount of the Sn substitution, while the increase in α to 1.30 for $x = 0.3$ shows shortened ON states. This trend of change in α shows the opposite behavior for GRAY states, *i.e.*, $\alpha = 0.99$ for $x = 0$ to $\alpha = 1.32$ for $x = 0.1$, indicating the suppression of GRAY states. On the other hand, the GRAY state kinetics of the $CsPb_{1-x}Sn_xBr_3$ QDs from $x = 0.1$ and $x = 0.3$ change moderately, especially at shorter times. Interestingly, α for OFF times in the Sn-substituted $CsPb_{1-x}Sn_xBr_3$ QDs decreases from 1.34 (for $x = 0.0$) to 0.80 (for $x = 0.3$) with increasing amount of Sn, which in turn shows the enhanced OFF durations in the later. It is important to mention that the 'α' and truncation observed to be different for individual emitters as compared to the sum over number of the particles (ensemble average) used to construct ($P(t)$) in Fig. 3(g–i). To visualize the extent of variation in α and truncation time, $P(t)$ curves for individual emitters for all three samples were fitted to the same function and the resulting parameter values are used to create the shadow which is overlaid over each $P(t)$ plot.

Table 1 Fitting parameters determined by the truncated power law fit to the data shown in Fig. 3(g–i)

	ON		GRAY		OFF	
$CsPb_{1-x}Sn_xBr_3$ ($x =$)	α	t_c (s)	α	t_c (s)	α	t_c (s)
0.0	1.01	0.85	0.99	3.70	1.34	0.40
0.1	0.73	2.77	1.32	0.42	1.47	0.32
0.3	1.30	0.47	1.21	2.44	0.80	0.94

Proposed mechanism: photoblinking and lifetime analysis

To explain the above results on the photophysical behaviour of the $CsPb_{1-x}Sn_xBr_3$ QDs, we have proposed a mechanism as illustrated in Fig. 4a. Intra-band trap states in the $CsPbBr_3$ NCs have been suggested by various groups due to the uncoordinated lead in LHPs.[40,42–44] Considering this, the scheme demonstrates that photo-generated electrons in the C.B. get trapped at the intra band electronic states, leading to the formation of trions in the $CsPb_{1-x}Sn_xBr_3$ ($x = 0$) QDs.[45] When these trap states are inactive, excitons undergo radiative recombination, while nonradioactive losses dominate when the traps become active.[46] Thus the recombination of these trions is unstable and active trap states lead to non-radiative emission. On incorporation of Sn in the $CsPb_{1-x}Sn_xBr_3$ QDs, the trap states are capable of capturing the photogenerated hot electrons (carriers prior to their cooling) of Sn energized by deactivation of trions at the Pb center.[45–50] These hot electrons occupy the Pb trap states, which in turn are no longer available for C.B. electrons. Thus, reduction in the C.B. electron transition to the Pb trap states results in increased radiative recombination and hence PLQY enhancement. Indeed, these recombination processes happen simultaneously within every individual entity, reflecting trap state's dynamic nature caused by movement of charge carriers and ion migration.[46,51] On the other hand, a further increase in the Sn content in the $CsPb_{1-x}Sn_xBr_3$ QDs (*i.e.*, for $x = 0.3$) brings them in proximity and undesired interactions among charge carriers which results in non-radiative recombination and lowering of PL.[52–54]

This proposed mechanism of filling trap states by Sn hot electrons not only explain our observations on photoblinking behavior of the $CsPb_{1-x}Sn_xBr_3$ QDs (Fig. 2), but also explain previously reported trend in PL emission.[19,26,27,55,56] For instance, in the case of Li doping, the introduction of a new energy level reported to prevent charge carrier trapping, while Na doping reduces charge carrier trap states through structural

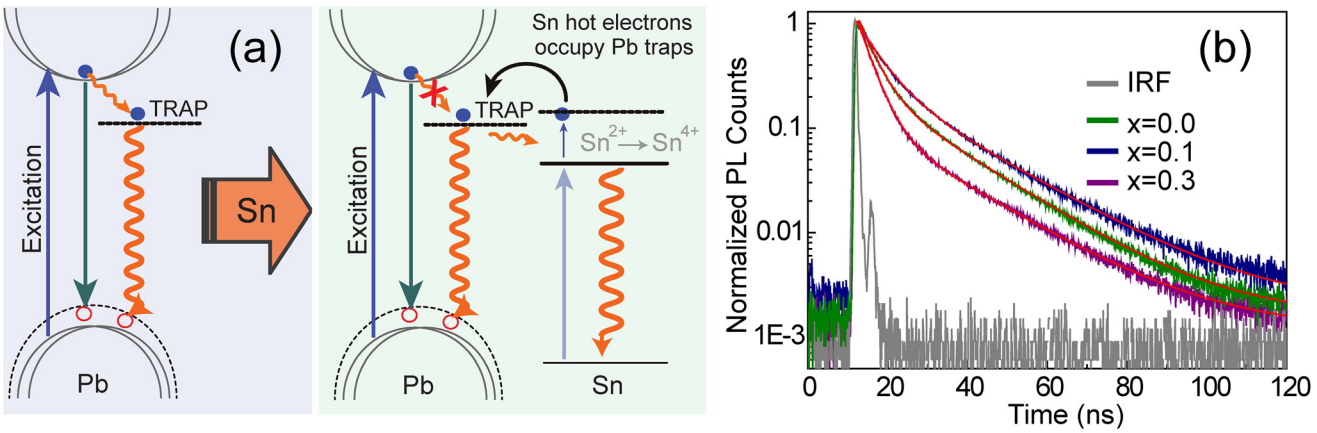

Fig. 4 (a) Schematic diagram of the proposed PL mechanism involving two energy states. In the left panel for $x = 0$, the excited electrons transfer to the trap state which is short lived and relaxes mainly non-radiatively (solid wavy line), and the presence of Sn in the vicinity of Pb fills the trap states with hot electrons generated due to photo-excitation and energized by the trap state relaxations. The solid lines symbolize excitation and radiative relaxations, while the curved arrows show electron transfers. PL decay curves (b) for ensembles of the $CsPb_{1-x}Sn_xBr_3$ QDs of varying 'x' values. These curves were fitted to the bi-exponential function, the fitting parameters of which are depicted in Table 2.

This journal is © The Royal Society of Chemistry 2025

Published on 17 January 2025. Downloaded on 2/15/2026 1:56:55 AM.

Table 2 Average lifetimes and radiative and non-radiative decay rates of the $CsPb_{1-x}Sn_xBr_3$ perovskites obtained using bi-exponential fitting to the decay curves shown in Fig. 4b

$CsPb_{1-x}Sn_xBr_3$ (x =)	PLQY (%)	τ_1 (ns)	α_1	τ_2 (ns)	α_2	$\tau_{avg} = \sum_i \frac{\alpha_i \tau_i^2}{\alpha_i \tau_i} (ns)$	$k_R = \frac{QY}{\tau_{avg}} (s^{-1})$	$k_{NR} = \frac{1}{\tau_{avg}} - k_R (s^{-1})$
0.0	71	3.8	0.76	17.8	0.24	12.15	5.8×10^7	2.3×10^7
0.1	89	5.5	0.71	19.9	0.29	14.08	6.3×10^7	0.7×10^7
0.3	53	3.5	0.89	19.1	0.11	9.78	5.4×10^7	4.8×10^7

improvements.[55,56] These observations can be explained by our proposed mechanism in which photogenerated hot electrons from Sn fill Pb-related trap states, enhancing radiative recombination. This is also supported by another study that Sn doping does not introduce any new recombination channels in this system.[27] Nonetheless, the aforementioned observations are further complemented by the excited-state lifetime measurements which were carried out under 405 nm excitation. Decay curves for the three different compositions of the $CsPb_{1-x}Sn_xBr_3$ QDs at their corresponding λ_{max}^{PL} are shown in Fig. 4b. The decay curves are non-exponential, indicating more than one emissive state in these QDs. The observed PL decays fitted well to the bi-exponential function and the fitting parameters for all three compositions used in this study are listed in Table 2.

The shorter lifetime components were determined as 3.8 ns (0.76), 5.5 ns (0.71) and 3.5 ns (0.89) for x = 0, 0.1, and 0.3 respectively, where the values given in the parentheses show intensity weighted fractions. On the other hand, the longer component varies from 17.8 ns (0.24), 19.9 ns (0.29) and 19.1 ns (0.11) with increasing x in the order of 0, 0.1 and 0.3. The shorter component of the lifetime assigned to the emission corresponds to the fast mixing of charged and neutral states, *i.e.*, GARY states, while the longer component is interpreted as neutral emissive, *i.e.*, ON states, respectively. An average excited-state lifetime of $CsPb_{1-x}Sn_xBr_3$ first increased from 12.1 ns (x = 0) to 14.0 ns (x = 0.1) and then decreased to 9.7 ns (x = 0.3) on further increase in the Sn content. Furthermore, to confer the impact of Sn content on the radiative (k_R) and non-radiative (k_{NR}) recombination rates, we evaluated k_R and k_{NR} rates from the PLQYs and PL lifetimes of the $CsPb_{1-x}Sn_xBr_3$ QDs using the expressions presented in Table 2. It is noted that, for x = 0 to x = 0.1, k_R increases marginally while decreasing k_{NR} is more prominent (decreased threefold). Thus, the incorporation of Sn in suitable amount has led to the suppression of non-radiative recombination and yields a high PLQY. Conversely, for x = 0.3, k_{NR} increases to twice that of k_{NR} at x = 0 and almost seven times that of k_{NR} at x = 0.1. This in turn shows that the increased PLQY in $CsPb_{0.9}Sn_{0.1}Br_3$ is mainly due to decreased non-radiative recombination, consistent with the GRAY state suppression for the x = 0.1 fraction of Sn. Similarly, enhanced non-radiative rates for x = 0.3 are well in agreement with the frequent 'OFF' states observed in Fig. 2 and 3. It has been shown that the fast-decaying PL of the Sn-based systems originates from both band-edge states and shallow states due to inherent defect sites.[27,57,58] The susceptibility of Sn to get oxidized leads these Sn-rich materials to exhibit significantly higher defect state densities.[16,18] The two processes, *i.e.*, trion recombination and Sn oxidation, may be considered as an independent phenomenon, counterbalancing each other retarding effects on the PLQY of $CsPb_{1-x}Sn_xBr_3$. Excess of the Sn hot carrier retards the lifetime of the entities in the trap state, contributing to the decline in the PLQY for x = 0.3. Alternatively, the decreased lifetime suggests that the excess of Sn could increase free exciton emission decay, potentially resulting from non-radiative energy transfer to the trap states.[27] These results are consistent with the scheme provided in Fig. 4a and well in agreement with the photoblinking behavior that provides insights into the trend of the PLQY observed for mixed metal $CsPb_{1-x}Sn_xBr_3$ perovskite QDs.

Conclusion

We report the first single-particle level study on 6–9 nm $CsPb_{1-x}Sn_xBr_3$ QDs, where x = 0, 0.1 and 0.3. These QDs show narrow and single-peak PL emission centered between 498 nm and 506 nm. The PLQY first increases up to x = 0.1 and then decreases on further increasing the amount of Sn. To understand this unusual PLQY trend, we have studied single-particle photoblinking behaviour of compositionally different but structurally similar QDs at millisecond time resolution. Real-time PL trajectories for these QDs have been statistically analyzed to obtain the durations and fractions of the ON, GRAY and OFF states. Our results show that the PLQY of the $CsPb_{0.9}Sn_{0.1}Br_3$ QDs is higher than that of the $CsPbBr_3$ QDs due to the suppression of GRAY states caused by the photogenerated hot electrons present in the Sn energy states. These hot electrons eventually occupy the trap states on the Pb center and inhibit the transition of excited electrons from the conduction band (C.B.) to the non-radiative recombination centers. This in turn leads to a higher PLQY through enhanced radiative recombination. Upon increasing the Sn content (*i.e.* x = 0.3), the PLQY decreases due to increased non-radiative recombination likely due to the close proximity of Sn ions. Additionally, the susceptibility of Sn to get oxidized leads these Sn-rich materials to exhibit significantly higher defect states, which further enhances non-radiative transitions. This combined study of PLQY, carrier lifetimes and photoblinking provides an opportunity to modulate the excitonic properties and charge carrier dynamics of mixed metal halide perovskites. In particular, this study presents insight into the role of Sn as a tool to optimize radiative recombination processes

Published on 17 January 2025. Downloaded on 2/15/2026 1:56:55 AM.

which can be useful in designing halide perovskite-based efficient LEDs and solar cells.

Author contributions

A. A. and D. K. S. conceived the idea and designed the research. A. A. and A. Y. synthesized the materials and performed bulk experiments. A. A. performed microscopy and data analysis. A. A., P. V. and D. K. S. contributed to manuscript writing; all authors approved the final manuscript.

Data availability

Materials and synthesis methodology, EDS spectra and data table of the $CsPb_{1-x}Sn_xBr_3$ QDs, Tauc plot of the $CsPb_{1-x}Sn_xBr_3$ QDs, home-built spectral imaging setup, histogram of the spatial distribution of PL, examples of the intensity traces of the $CsPb_{1-x}Sn_xBr_3$ QDs, and criteria for determining ON, GRAY, and OFF states (PDF).

Conflicts of interest

The authors declare no conflicts of interest.

Acknowledgements

D. K. S. acknowledges financial support from the SERB-DST Project No.: SRG/2021/000004. A. A. and D. K. S. acknowledge MANIT Bhopal for funding and infrastructure facilities, as well as the Department of Chemistry for its constant support. We thank Prof. A. Chowdhury (IITB) for his critical comments and valuable suggestions on the photoblinking analysis.

References

1 F. Hao, C. C. Stoumpos, R. P. H. Chang and M. G. Kanatzidis, Anomalous band gap behavior in mixed Sn and Pb perovskites enables broadening of absorption spectrum in solar cells, *J. Am. Chem. Soc.*, 2014, **136**, 8094–8099.

2 H. Zhou, Qi Chen, G. Li, L. Song, S. Tze-bing, D. Hsin-Sheng, H. Ziruo and Y. Yang, Interface engineering of highly efficient perovskite solar cellsaccumbens, *Science*, 2014, **345**, 535–542.

3 M. Liu, M. B. Johnston and H. J. Snaith, Efficient planar heterojunction perovskite solar cells by vapour deposition, *Nature*, 2013, **501**, 395–398.

4 B. Yang, J. Chen, F. Hong, X. Mao, K. Zheng, S. Yang, Y. Li, T. Pullerits, W. Deng and K. Han, Lead-Free, Air-Stable All-Inorganic Cesium Bismuth Halide Perovskite Nanocrystals, *Angew. Chem., Int. Ed.*, 2017, **56**, 12471–12475.

5 N. Mondal, A. De and A. Samanta, Biexciton Generation and Dissociation Dynamics in Formamidinium- and Chloride-Doped Cesium Lead Iodide Perovskite Nanocrystals, *J. Phys. Chem. Lett.*, 2018, **9**, 3673–3679.

6 A. Soosaimanickam, P. J. Rodríguez-Cantó, J. P. Martínez-Pastor and R. Abargues, *Recent advances in synthesis, surface chemistry of cesium lead-free halide perovskite nanocrystals and their potential applications*, Elsevier, 2020, pp. 157–228.

7 H. C. Wang, Z. Bao, H. Y. Tsai, A. C. Tang and R. S. Liu, Perovskite Quantum Dots and Their Application in Light-Emitting Diodes, *Small*, 2018, **14**, 1–23.

8 Z. Shen, S. Zhao, D. Song, Z. Xu, B. Qiao, P. Song, Q. Bai, J. Cao, G. Zhang and W. Swelm, Improving the Quality and Luminescence Performance of All-Inorganic Perovskite Nanomaterials for Light-Emitting Devices by Surface Engineering, *Small*, 2020, **16**, 1–28.

9 A. Dutta, R. K. Behera, P. Pal, S. Baitalik and N. Pradhan, Near-Unity Photoluminescence Quantum Efficiency for All $CsPbX_3$ (X = Cl, Br, and I) Perovskite Nanocrystals: A Generic Synthesis Approach, *Angew. Chem., Int. Ed.*, 2019, **58**, 5552–5556.

10 Y. Shi, J. Xi, T. Lei, F. Yuan, J. Dai, C. Ran, H. Dong, B. Jiao, X. Hou and Z. Wu, Rubidium Doping for Enhanced Performance of Highly Efficient Formamidinium-Based Perovskite Light-Emitting Diodes, *ACS Appl. Mater. Interfaces*, 2018, **10**, 9849–9857.

11 L. Protesescu, S. Yakunin, M. I. Bodnarchuk, F. Krieg, R. Caputo, C. H. Hendon, R. X. Yang, A. Walsh and M. V. Kovalenko, Nanocrystals of Cesium Lead Halide Perovskites ($CsPbX_3$, X = Cl, Br, and I): Novel Optoelectronic Materials Showing Bright Emission with Wide Color Gamut, *Nano Lett.*, 2015, **15**, 3692–3696.

12 E. P. Yao, Z. Yang, L. Meng, P. Sun, S. Dong, Y. Yang and Y. Yang, High-Brightness Blue and White LEDs based on Inorganic Perovskite Nanocrystals and their Composites, *Adv. Mater.*, 2017, **29**, 1–7.

13 Q. A. Akkerman, V. D'Innocenzo, S. Accornero, A. Scarpellini, A. Petrozza, M. Prato and L. Manna, Tuning the optical properties of cesium lead halide perovskite nanocrystals by anion exchange reactions, *J. Am. Chem. Soc.*, 2015, **137**, 10276–10281.

14 A. Goyal, S. McKechnie, D. Pashov, W. Tumas, M. Van Schilfgaarde and V. Stevanović, Origin of Pronounced Nonlinear Band Gap Behavior in Lead-Tin Hybrid Perovskite Alloys, *Chem. Mater.*, 2018, **30**, 3920–3928.

15 A. B. F. Vitoreti, S. Agouram, M. Solis De La Fuente, V. Munoz-Sanjosé, M. A. Schiavon and I. Mora-Seró, Study of the Partial Substitution of Pb by Sn in Cs-Pb-Sn-Br Nanocrystals Owing to Obtaining Stable Nanoparticles with Excellent Optical Properties, *J. Phys. Chem. C*, 2018, **122**, 14222–14231.

16 T. Handa, A. Wakamiya and Y. Kanemitsu, Photophysics of lead-free tin halide perovskite films and solar cells, *APL Mater.*, 2019, **7**, 1–12.

17 H. Xu, J. Duan, Y. Zhao, Z. Jiao, B. He and Q. Tang, 9.13%-Efficiency and stable inorganic $CsPbBr_3$ solar cells. Lead-

 This journal is © The Royal Society of Chemistry 2025

Published on 17 January 2025. Downloaded on 2/15/2026 1:56:55 AM.

free $CsSnBr_{3-x}I_x$ quantum dots promote charge extraction, *J. Power Sources*, 2018, **399**, 76–82.

18 G. Nasti and A. Abate, Tin Halide Perovskite ($ASnX_3$) Solar Cells: A Comprehensive Guide toward the Highest Power Conversion Efficiency, *Adv. Energy Mater.*, 2020, **10**, 1–16.

19 D. Ricciarelli, D. Meggiolaro, F. Ambrosio and F. De Angelis, Instability of tin iodide perovskites: Bulk p-doping versus surface tin oxidation, *ACS Energy Lett.*, 2020, **5**, 2787–2795.

20 H.-C. Wang, W. Wang, A.-C. Tang, H.-Y. Tsai, Z. Bao, T. Ihara, N. Yarita, H. Tahara, Y. Kanemitsu, S. Chen and R.-S. Liu, High-Performance $CsPb_{1-x}Sn_xBr_3$ Perovskite Quantum Dots for Light-Emitting Diodes, *Angew. Chem.*, 2017, **129**, 13838–13842.

21 Y. Hu, F. Bai, X. Liu, Q. Ji, X. Miao, T. Qiu and S. Zhang, Bismuth Incorporation Stabilized α-$CsPbI_3$ for Fully Inorganic Perovskite Solar Cells, *ACS Energy Lett.*, 2017, **2**, 2219–2227.

22 X. Shen, Y. Zhang, S. V. Kershaw, T. Li, C. Wang, X. Zhang, W. Wang, D. Li, Y. Wang, M. Lu, L. Zhang, C. Sun, D. Zhao, G. Qin, X. Bai, W. W. Yu and A. L. Rogach, Zn-Alloyed CsPbI 3 Nanocrystals for Highly Efficient Perovskite Light-Emitting Devices, *Nano Lett.*, 2019, **19**, 1552–1559.

23 P. N. Tran, H. H. Phan, T. N. Luu, Q. H. Tran and T. T. Duong, Optimizing the single-source flash thermal evaporation process of Zn-doped $CsPbBr_3$ films for enhanced performance in perovskite LEDs, *Appl. Phys. A: Mater. Sci. Process.*, 2024, **130**, 1–7.

24 A. L. Abdelhady, M. I. Saidaminov, B. Murali, V. Adinolfi, O. Voznyy, K. Katsiev, E. Alarousu, R. Comin, I. Dursun, L. Sinatra, E. H. Sargent, O. F. Mohammed and O. M. Bakr, Heterovalent Dopant Incorporation for Bandgap and Type Engineering of Perovskite Crystals, *J. Phys. Chem. Lett.*, 2016, **7**, 295–301.

25 Q. A. Akkerman, D. Meggiolaro, Z. Dang, F. De Angelis and L. Manna, Fluorescent Alloy $CsPbxMn_{1-x}I_3$ Perovskite Nanocrystals with High Structural and Optical Stability, *ACS Energy Lett.*, 2017, **2**, 2183–2186.

26 S. Kundu, D. Zhang, A. M. Askar, E. G. Moloney, M. M. Adachi, A. Nadeem, S. Moradi, V. Yeddu, A. L. Abdelhady, O. Voznyy and M. I. Saidaminov, Bismuth Stabilizes the α-Phase of Formamidinium Lead Iodide Perovskite Single Crystals, *ACS Mater. Lett.*, 2022, **4**, 707–712.

27 X. Zhang, W. Cao, W. Wang, B. Xu, S. Liu, H. Dai, S. Chen, K. Wang and X. W. Sun, Efficient light-emitting diodes based on green perovskite nanocrystals with mixed-metal cations, *Nano Energy*, 2016, **30**, 511–516.

28 J. Deng, H. Wang, J. Xun, J. Wang, X. Yang, W. Shen, M. Li and R. He, Room-temperature synthesis of excellent-performance $CsPb_{1-x}Sn_xBr_3$ perovskite quantum dots and application in light emitting diodes, *Mater. Des.*, 2020, **185**, 1–13.

29 G. Yuan, D. E. Gómez, N. Kirkwood, K. Boldt and P. Mulvaney, Two Mechanisms Determine Quantum Dot Blinking, *ACS Nano*, 2018, **12**, 3397–3405.

30 D. P. Fromm, S. T. Johnson, A. Gallagher and D. J. Nesbitt, Modeling distributed kinetics in isolated semiconductor quantum dots, *Phys. Rev. B: Condens. Matter Mater. Phys.*, 2003, **67**, 1–15.

31 C. Galland, Y. Ghosh, A. Steinbrück, M. Sykora, J. A. Hollingsworth, V. I. Klimov and H. Htoon, Two types of luminescence blinking revealed by spectroelectrochemistry of single quantum dots, *Nature*, 2011, **479**, 203–207.

32 T. Takagi, S. Omagari and M. Vacha, Suppression of blinking in single $CsPbBr_3$ perovskite nanocrystals through surface ligand exchange, *Phys. Chem. Chem. Phys.*, 2023, **25**, 19004–19012.

33 D. K. Sharma, S. Hirata, V. Biju and M. Vacha, Stark Effect and Environment-Induced Modulation of Emission in Single Halide Perovskite Nanocrystals, *ACS Nano*, 2019, **13**, 624–632.

34 N. Pathoor and A. Chowdhury, Spatially Correlated Blinking of Perovskite Micro-crystals: Deciphering Effective Modes of Communication between Distal Photoexcited Carriers, *ACS Photonics*, 2023, **10**, 49–57.

35 A. Swarnkar, R. Chulliyil, V. K. Ravi, M. Irfanullah, A. Chowdhury and A. Nag, Colloidal CsPbBr 3 Perovskite Nanocrystals: Luminescence beyond Traditional Quantum Dots, *Angew. Chem.*, 2015, **127**, 15644–15648.

36 D. K. Sharma, S. Hirata, L. Bujak, V. Biju, T. Kameyama, M. Kishi, T. Torimoto and M. Vacha, Single-particle spectroscopy of I-III-VI semiconductor nanocrystals: Spectral diffusion and suppression of blinking by two-color excitation, *Nanoscale*, 2016, **8**, 13687–13694.

37 Y. Cao, D. Wu, P. Zhu, D. Shan, X. Zeng and J. Xu, Down-shifting and anti-reflection effect of $cspbbr_3$ quantum dots/multicrystalline silicon hybrid structures for enhanced photovoltaic properties, *Nanomaterials*, 2020, **10**, 775.

38 P. P. Jha and P. Guyot-sionnest, Trion Decay in Colloidal Quantum Dots, *ACS Nano*, 2009, **3**, 1011–1015.

39 D. E. Go, J. Van Embden, P. Mulvaney, M. J. Ferne and H. Rubinsztein-Dunlop, Exciton - Trion Transitions in Single CdSe–CdS Core–Shell Nanocrystals, *ACS Nano*, 2009, **3**, 2281–2287.

40 N. Yarita, H. Tahara, M. Saruyama, T. Kawawaki, R. Sato, T. Teranishi and Y. Kanemitsu, Impact of Postsynthetic Surface Modification on Photoluminescence Intermittency in Formamidinium Lead Bromide Perovskite Nanocrystals, *J. Phys. Chem. Lett.*, 2017, **8**, 6041–6047.

41 J. J. Peterson and D. J. Nesbitt, Modified power law behavior in quantum dot blinking: A novel role for biexcitons and auger ionization, *Nano Lett.*, 2009, **9**, 338–345.

42 B. A. Koscher, J. K. Swabeck, N. D. Bronstein and A. P. Alivisatos, Essentially Trap-Free $CsPbBr_3$ Colloidal Nanocrystals by Postsynthetic Thiocyanate Surface Treatment, *J. Am. Chem. Soc.*, 2017, **139**, 6566–6569.

43 T. Ahmed, S. Seth and A. Samanta, Boosting the Photoluminescence of $CsPbX_3$ (X = Cl, Br, I) Perovskite Nanocrystals Covering a Wide Wavelength Range by Postsynthetic Treatment with Tetrafluoroborate Salts, *Chem. Mater.*, 2018, **30**, 3633–3637.

Published on 17 January 2025. Downloaded on 2/15/2026 1:56:55 AM.

44 S. Seth, T. Ahmed and A. Samanta, Photoluminescence Flickering and Blinking of Single CsPbBr 3 Perovskite Nanocrystals: Revealing Explicit Carrier Recombination Dynamics, *J. Phys. Chem. Lett.*, 2018, **9**, 7007–7014.
45 T. Ahmed, S. Seth and A. Samanta, Mechanistic Investigation of the Defect Activity Contributing to the Photoluminescence Blinking of $CsPbBr_3$ Perovskite Nanocrystals, *ACS Nano*, 2019, **13**, 13537–13544.
46 M. Gerhard, B. Louis, R. Camacho, A. Merdasa, J. Li, A. Kiligaridis, A. Dobrovolsky, J. Hofkens and I. G. Scheblykin, Microscopic insight into non-radiative decay in perovskite semiconductors from temperature-dependent luminescence blinking, *Nat. Commun.*, 2019, **10**, 1–12.
47 B. Yang and K. Han, Charge-Carrier Dynamics of Lead-Free Halide Perovskite Nanocrystals, *Acc. Chem. Res.*, 2019, **52**, 3188–3198.
48 A. Dey, *et al.*, State of the Art and Prospects for Halide Perovskite Nanocrystals, *ACS Nano*, 2021, **15**, 10775–10981.
49 H. Zhu, Y. Yang and T. Lian, Multiexciton annihilation and dissociation in quantum confined semiconductor nanocrystals, *Acc. Chem. Res.*, 2013, **46**, 1270–1279.
50 O. E. Semonin, J. M. Luther, S. Choi, H.-Y. Chen, G. Jianbo, A. J. Nozik and M. C. Beard, Peak External Photocurrent Quantum Efficiency Exceeding 100% via MEG in a Quantum Dot Solar Cell, *Science*, 2011, **334**, 1530–1534.
51 K. Wei, Y. Liu, H. Yang, X. Cheng and T. Jiang, Large range modification of exciton species in monolayer WS_2, *Appl. Opt.*, 2016, **55**, 6251–6255.
52 A. Wang, Y. Guo, F. Muhammad and Z. Deng, Controlled Synthesis of Lead-Free Cesium Tin Halide Perovskite Cubic Nanocages with High Stability, *Chem. Mater.*, 2017, **29**, 6493–6501.
53 D. K. Sharma, S. Hirata, L. Bujak, V. Biju, T. Kameyama, M. Kishi, T. Torimoto and M. Vacha, Influence of Zn on the photoluminescence of colloidal (AgIn): $XZn_{2(1-x)}S_2$ nanocrystals, *Phys. Chem. Chem. Phys.*, 2017, **19**, 3963–3969.
54 D. K. Sharma, S. Hirata and M. Vacha, Single-particle electroluminescence of $CsPbBr_3$ perovskite nanocrystals reveals particle-selective recombination and blinking as key efficiency factors, *Nat. Commun.*, 2019, **10**, 1–5.
55 H. Zalrhi, M. Ouafi, M. Regragui, B. M. Soucase, F. Baig, Y. H. Khattak, U. Shafi, M. Abd-lefdil and L. Atourki, Improving photoluminescence properties and reducing recombination of $CsPbBr_3$ perovskite through lithium doping, *RSC Adv.*, 2024, **14**, 15048–15057.
56 S. Li, Z. Shi, F. Zhang, L. Wang, Z. Ma, D. Yang, Z. Yao, D. Wu, T. Xu, Y. Tian, Y. Zhang, C. Shan and X. J. Li, Sodium Doping-Enhanced Emission Efficiency and Stability of $CsPbBr_3$ Nanocrystals for White Light-Emitting Devices, *Chem. Mater.*, 2019, **31**, 3917–3928.
57 Z. Xiao, Y. Zhou, H. Hosono and T. Kamiya, Intrinsic defects in a photovoltaic perovskite variant Cs_2SnI_6, *Phys. Chem. Chem. Phys.*, 2015, **17**, 18900–18903.
58 F. Deschler, M. Price, S. Pathak, L. E. Klintberg, D. D. Jarausch, R. Higler, S. Hüttner, T. Leijtens, S. D. Stranks, H. J. Snaith, M. Atatüre, R. T. Phillips and R. H. Friend, High photoluminescence efficiency and optically pumped lasing in solution-processed mixed halide perovskite semiconductors, *J. Phys. Chem. Lett.*, 2014, **5**, 1421–1426.

This journal is © The Royal Society of Chemistry 2025